AIChE

Modeling Multicomponent Adsorption of Monoclonal Antibody Charge Variants in Cation Exchange Columns

Yinying Tao, Nianyun Chen, and Giorgio Carta
Dept. of Chemical Engineering, University of Virginia, Charlottesville, VA 22904

Gisela Ferreira and David Robbins
MedImmune, One MedImmune Way, Gaithersburg, MD 20878

DOI 10.1002/aic.13718
Published online December 29, 2011 in Wiley Online Library (wileyonlinelibrary.com).

Transport models are developed for the adsorption of monoclonal antibody charge variants in cation exchange columns for two different matrices: UNOsphere S, which has a macroporous architecture, and Capto S, which contains charged dextran polymers grafted to an agarose matrix. The UNOsphere S protein adsorption kinetics is described by a macropore diffusion model with effective pore diffusivity $D_e = 8.3 \times 10^{-8}$ cm^2/s, which successfully predicts resolution of charge variants by frontal analysis at residence times, L/u, between 0.9 and 5.4 min. The Capto S adsorption kinetics is very fast for individual charge variants and for coadsorption of their mixtures, but is dramatically slower for sequential adsorption, when a more strongly bound variant displaces a more weakly bound one. A Maxwell-Stefan model assuming single-file diffusion predicts, in agreement with experiments, poor resolution of charge variants by frontal analysis even at long residence times as a result of highly hindered counterdiffusion. © 2011 American Institute of Chemical Engineers *AIChE J,* 58: 2503–2511, 2012
Keywords: monoclonal antibody charge variants, ion exchange, multicomponent adsorption kinetics, mass transfer modeling, diffusion

Introduction

The chromatographic separation of the charge variants of monoclonal antibodies (mAbs) and other proteins is an important industrial problem.[1] Such variants can be formed as a result of post-translational modifications such as deamidation, which transforms asparagine and glutamine residues into negatively charged aspartic and glutamic acid residues. As the resulting isoforms can have reduced activity and/or stability, their separation is often desirable. Cation exchange chromatography is ideally suited for this purpose since the separation is due to electrostatic interactions with the stationary phase, which, in turn, are affected by the protein charge.

While several authors have demonstrated resolution of mAb charge variants using high-performance analytical cation exchange columns[2–4] our prior work has focused on stationary phases suitable for low-pressure chromatography at the process scale and at high protein loads.[5–6] Two different stationary phases were tested in the prior work for their ability to adsorb and separate the deamidated isoforms of a mAb. The first of these stationary phases, UNOsphere S (Bio-Rad Laboratories, Hercules, CA), is a macroporous, polymer-based cation exchanger, while the second, Capto S (GE Healthcare, Piscataway, NJ) is an agarose matrix with charged dextran grafts. Although both matrices exhibited substantial selectivity, showing a distinct preference for binding the less deamidated forms, binding capacity and adsorption kinetics were strikingly different between the two gels. For UNOsphere S, the binding capacity was found to be limited by the pore surface area and the kinetics of adsorption to be controlled by the slow diffusion of mAb molecules in the particle macropores. Thus, a pore diffusion model with instantaneous exchange of one adsorbed variant for another was found to be consistent with the data. This model could accurately predict the adsorption kinetics for single-component and multicomponent systems regardless of the sequence of exposure of the particle to the different components; i.e., both for coadsorption of multiple isoforms and for sequential adsorption, when a more strongly adsorbed variant added later displaced a more weakly bound species that had previously been adsorbed.

For Capto S, on the other hand, the binding capacity for each of the variants was much higher than that for UNOsphere S, and this result was attributed to the improved access to negatively charged functional groups provided by the dextran grafts that appear to function as surface extenders. The adsorption kinetics was also much faster than that observed for UNOsphere S, but only for the cases of adsorption of individual variants or for simultaneous coadsorption of multiple variants on a clean particle. In contrast, sequential adsorption (addition of more strongly bound variant to beads already containing the weakly bound form) was instead dramatically slower likely as a result of extremely slow mass transfer. The faster kinetics observed for the single-component adsorption and simultaneous coadsorption

Correspondence concerning this article should be addressed to G. Carta at gc@virginia.edu.
Current address for Yinying Tao: Biogen Idec, Inc., 5000 Davis Drive, Research Triangle Park, NC 27709.
Current Address for Nianyun Chen: Shire, 700 Main St. Cambridge, MA 02139.

cases was attributed to interactions with the charged dextran grafts through a mechanism commonly referred to as "solid" or "adsorbed phase" diffusion. The latter occurs, for example, when adsorbed molecules can "hop" from one adsorption site to another or continuously migrate along a surface or in a gel phase.[7–8] Although either hopping or migration rates can be expected to be low, resulting in low mobility, in both cases the driving force, being proportional to the adsorbed protein concentration, is large, resulting in rapid overall mass transfer kinetics.[9] Obviously, such a mechanism can be expected to depend on the composition of the adsorbed phase and on the direction of transport. Thus, while a Fickian diffusion model with an adsorbed concentration driving force could describe the Capto S results for the single component and coadsorption cases, it completely failed to predict the much slower sequential adsorption behavior, likely as a result of a highly hindered counterdiffusion process within the dextran grafts.

We also recently confirmed the vastly different behavior of UNOsphere S and Capto S at the microscopic level using confocal laser scanning microscopy (CLSM) to visualize the movement of fluorescently labeled deamidated mAb isoforms within the particles.[10] UNOsphere S showed sharp intraparticle concentration profiles for one-component adsorption consistent with the shrinking-core model, and displacement of a more weakly adsorbed isoform by a more strongly adsorbed one during binary coadsorption, which resulted in a temporary accumulation of the more weakly bound variant in the center of the particle. Displacement within the particle was also observed for sequential adsorption of the two variants on UNOsphere S with a sharp front of the more strongly bound variant progressing toward the particle center. Capto S, on the other hand, showed smooth concentration profiles within the particle and very rapid approach to equilibrium for both one-component and binary coadsorption cases on time scales similar to those observed in batch adsorption experiments. However, only a small percentage of the weakly bound variant was desorbed in the sequential adsorption case in a manner both qualitatively and quantitatively consistent with the batch sequential adsorption results.

From a practical viewpoint, the focus of industrial interest is on predicting the behavior of chromatography columns, which requires a description of both equilibrium and mass-transfer effects. This is relatively straightforward as long as a suitable model is available. Since in a typical column process, coadsorption and displacement of one adsorbed variant by another occur simultaneously in different parts of the column, the model must be able to accurately describe adsorption kinetics regardless of the direction of transport within the particles. The objective of this work is, thus, twofold. The first objective is to extend and validate experimentally the previously developed pore diffusion model for columns packed with UNOsphere S. The second objective is to develop a new model capable of describing the complex adsorption kinetics of Capto S and extend this new model to the prediction of column behavior.

Materials and Methods

UNOsphere S and Capto S were obtained from Bio-Rad Laboratories (Hercules, CA,) and GE Healthcare (Piscataway, NJ), respectively. UNOsphere S is polymer-based and has an open macroporous structure with an apparent pore radius around 60 nm based on the exclusion limit determined by inverse size exclusion chromatography (iSEC) as described by Hagel et al.[11] Capto S consists of agarose grafted with ionically functionalized dextran polymers. Based on iSEC, the apparent pore radius of Capto S at low ionic strength (20 mmol/L Na^+, which corresponds to a conductivity of about 1.7 mS/cm at 25°C) is about 5 nm, which is very similar to the mAb hydrodynamic radius. Because the pores are too small to permit ready diffusion of the mAb in the liquid phase, it is apparent that molecular diffusion in Capto S must occur through continuous interactions with the charged dextran graft layer. Mean particle diameters were 75 and 89 μm for UNOsphere S and Capto S, respectively.[5]

As described by Tao et al.[5] different fractions of a deamidated mAb mixture were separated by cation exchange chromatography using a Source 30S column from GE Healthcare (Piscataway, NJ). Fraction 2, which is more deamidated and has lower net positive charge, and Fraction 3, which is less deamidated, were used in this work. Experiments were carried out with the purified variants as well as with mixtures of the two variants in a 10 mmol/L Na_2HPO_4 buffer at pH 7.5. At this pH both stationary phases preferentially adsorbed the less deamidated species, Fraction 3.

Frontal loading column experiments were done by flow-packing each stationary phase in 5 mm dia. Tricorn™ columns from GE Healthcare with lengths between 23 and 55 mm, operated at flow rates between 0.2×10^{-3} and 1.2×10^{-3} L/min (corresponding to superficial velocities between 61 and 370 cm/h). The corresponding residence times were between 0.9 and 5.4 min. An ÄKTA Explorer 10 unit from GE Healthcare was used to provide flow of equilibration buffer, protein load, and elution buffer (10 mmol/L Na_2HPO_4 + 1 mol/L NaCl at pH 7.5). Eluent samples were collected with the ÄKTA fraction collector and analyzed by cation exchange chromatography as described in Tao et al.[5] All experiments were conducted at room temperature, 23 ± 2°C.

Results

Adsorption equilibrium

Adsorption equilibrium data were obtained for each mAb fraction and their mixtures by Tao et al.[5] and are described by the steric mass action model of Brooks and Cramer.[12]

Accordingly, equilibrium is described by the following equation

$$C_i = \frac{q_i/q_0}{\frac{K_{e,i}q_0^{z_i-1}}{C_I^{z_i}}\left[1-\sum_j\left(z_j+\sigma_j\right)\frac{q_j}{q_0}\right]^{z_i}} \tag{1}$$

where C_i is the protein solution phase concentration, q_i the adsorbed protein concentration, $K_{e,i}$ is the equilibrium constant describing the exchange of protein for a monovalent counterion, C_I is the concentration of counterions (Na^+, in our case), q_0 the concentration of ionogenic groups in the adsorbent, z_i is the protein binding charge, and σ_i is the steric hindrance factor. The latter describes the number of functional groups that are blocked by each bound protein molecule. Model parameters used in this work are summarized in Table 1. Note that, since adsorption is favorable and the solutions considered are dilute, we do not distinguish between protein molecules that are adsorbed and those that are merely held in the macropore fluid.

Table 1. SMA Isotherm Parameters based on Tao et al[5]

	UNOsphere S (q_0 =150 mmol/L)			Capto S (q_0 = 220 mmol/L)		
Fraction	K_e	z	σ	K_e	z	σ
2	3.7×10^{-2}	7.0	122	0.7×10^{-4}	8.3	69
3	15.4×10^{-2}	7.0	122	5.4×10^{-4}	8.3	69

Thus, in practice, q_i is essentially coincident with the total protein concentration in the particle.

Adsorption Kinetics and Column Behavior

Results for UNOsphere S

Figure 1 shows representative batch adsorption kinetics results obtained for UNOsphere S by Tao et al.[6] for single-component adsorption, coadsorption, and sequential adsorption. As seen from this figure, all three processes occur over similar time scales and in all three cases equilibrium is attained in about 6,000 s. Predictions are shown based on the pore diffusion model of Tao et al.[6] which assumes that the diffusion fluxes for each component are independent of the others and proportional to that component's concentration gradient in the pore fluid ∇c_i. Accordingly, the flux J_i, is given by

$$J_i = -D_{e,i}\nabla c_i \tag{2}$$

where D_{ei} is the effective pore diffusivity. Batch adsorption in spherical particles is then described by the following set of equations and boundary conditions:

$$\frac{\partial q_i}{\partial t} = \frac{D_{e,i}}{r^2}\frac{\partial}{\partial r}\left(r^2\frac{\partial c_i}{\partial r}\right) \tag{3}$$

$$\left.\frac{\partial c_i}{\partial r}\right|_{r=0} = 0 \tag{3a}$$

$$D_{e,i}\left.\frac{\partial c_i}{\partial r}\right|_{r=r_p} = k_{f,i}\left(C_i - c_i|_{r=r_p}\right) \tag{3b}$$

$$V\frac{dC_i}{dt} = -\frac{3V_M}{r_p}D_{e,i}\left.\frac{\partial c_i}{\partial r}\right|_{r=r_p} \tag{4}$$

$$C_i|_{t=0} = C_{0,i} \tag{4a}$$

where C_i is the protein concentration in the bulk liquid, q_i is the adsorbed protein concentration, is the external boundary layer mass-transfer coefficient, V and V_M, the solution and adsorbent volumes, respectively, and r_p the particle radius. q_i and c_i are assumed to be in equilibrium locally within the particle with their relationship expressed by Eq. 1. The model equations were solved numerically as discussed by Tao et al.[6] As seen in Figure 1, the pore diffusion model describes all three cases with an effective pore diffusivity $D_e = 8.3 \times 10^{-8}$ cm^2/s, and $k_f = 0.0015$ cm/s for both variants, both determined as described by Tao et al.[6] Similar values of both D_e and k_f are obtained for the two variants since their molecular size is essentially the same and their charge is very similar. The corresponding Biot number ($B_i = k_f r_p/D_e$) is around 70, indicating that the external resistance is negligible under these conditions.[13–14]

The column results are shown in Figures 2 and 3 for single-component and two-component adsorption, respectively, at different residence times. Plots are shown in terms of effluent protein concentration divided by the feed concentration, as a function of total protein loaded per unit column volume. For the single-component case, the breakthrough curve becomes shallower as the residence time decreases from 5.4 to 0.9 min. As a result, the dynamic binding capacity at 10% of breakthrough decreases from about 68 g/L at 5.4 min residence time to about 40 g/L at 0.9 min. For the two-component case (Figure 3), an overshoot or "roll-up" of the more weakly binding Fraction 2 is observed. This occurs as a result of reversible competitive binding of the two variants which causes Fraction 2 to accumulate downstream of the feed front in the column, only to be ultimately displaced by Fraction 3.[13–14] The breakthrough curves for the two-component case also become shallower as the residence time decreases, and the overshoot or "roll-up" of the more weakly binding Fraction 2 becomes less pronounced. On the other hand, even at 0.9 min residence time, Fraction 2 emerges from the column with substantial purity and attaining a peak concentration about 1.4 times the feed value. Figure 4 shows the results for different ratios of the two variants in the feed at a residence time of 0.9 min. Steeper curves are obtained at higher load ratios of Fraction 3 to Fraction 2, with Fraction 2 reaching a peak concentration of about 1.5 times the feed value. This improvement occurs because the higher relative concentration of Fraction 3 results in faster mass transfer and easier displacement of Fraction 2.

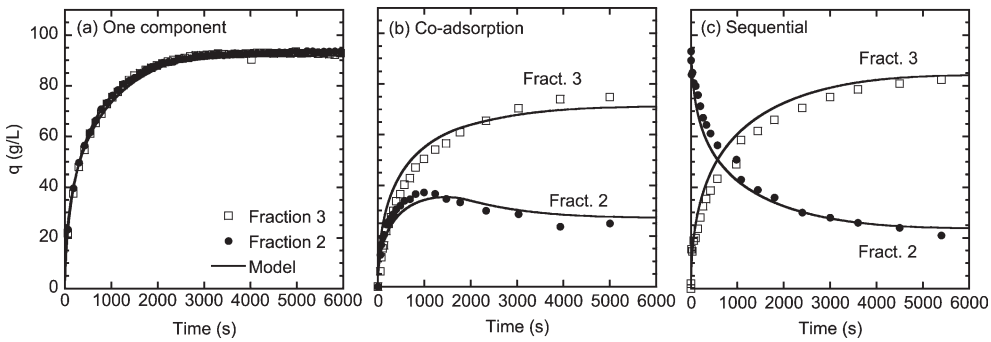

Figure 1. Batch adsorption kinetics of UNOsphere S.

(a) Single-component adsorption of mAb Fractions 2 and 3 from 1 g/L solutions, (b) coadsorption of mAb Fractions 2 and 3 from a solution containing 1 g/L of each variant, and (c) Sequential adsorption of Fraction 3 from a 1 g/L solution of Fraction 3 on particles pre-equilibrated in a 1 g/L solution of Fraction 2. Data are from Tao et al.[6] Lines show predictions of the pore diffusion model with $D_e = 8.3 \times 10^{-8}$ cm^2/s.

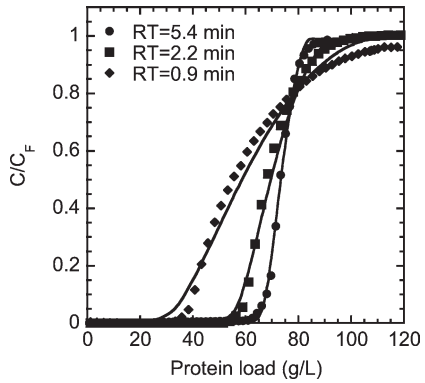

Figure 2. Single-component breakthrough curves of 2 g/L mAb Fraction 3 for a UNOsphere S column at different residence times (RT = *L/u*).

The column length was 55 mm. Lines show predictions of the pore diffusion model with $D_e = 8.3 \times 10^{-8}$ cm^2/s.

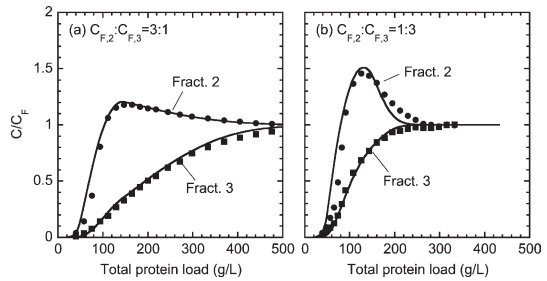

Figure 4. Two-component breakthrough curves of mixtures containing (a) 1.5 g/L of mAb Fraction 2 and 0.5 g/L of mAb Fraction 3, and (b) 0.5 g/L of mAb Fraction 2 and 1.4 g/L of mAb Fraction 3 for a UNOsphere S column at a 0.9 min residence time.

The column length was 23 mm. Lines show predictions of the pore diffusion model with $D_e = 8.3 \times 10^{-8}$ cm^2/s.

Modeling the column behavior requires coupling Eqs. 1 and 3 with material balances for the column. Assuming plug flow and neglecting axial dispersion, the latter can be written as follows

$$\varepsilon \frac{\partial C_i}{\partial t} + (1-\varepsilon)\frac{\partial \overline{q}_i}{\partial t} + u\frac{\partial C_i}{\partial x} = 0 \tag{5}$$

$$C_i|_{t=0} = 0, \quad \overline{q}_i|_{t=0} = 0, \quad C_i|_{x=0} = C_{F,i} \tag{5a}$$

$$\frac{\partial \overline{q}_i}{\partial t} = k_{f,i}\left(C_i - c_i|_{r=r_p}\right) \tag{6}$$

In these equations ϵ is the extraparticle porosity (assumed to be 0.3, based on the results in Tao et al.[5–6]), $\overline{q}$ the particle-averaged adsorbed concentration, x the axial coordinate, t the time, and $C_{F,i}$ the feed concentration. A numerical solution of these equations was obtained using finite differences as discussed by Carta and Lewus.[15] Model predictions are shown in Figures 2–4, using the parameters determined in the batch adsorption experiments, $D_e = 8.3 \times 10^{-8}$ cm^2/s and $k_f = 0.0015$ cm/s. Since Bi is large, the results are insensitive to the precise value of k_f. Thus, D_e is the main determinant of the effects of residence time. In fact, based on the large Bi, it is clear that a simplified model, neglecting the external resistance could be used with little error in lieu of the full model. Nevertheless, since the additional computational burden is minimal, the full model was used. Predictions with no adjustable parameters are quite accurate for both single- and two-component cases over a broad range of conditions indicating that the model provides an adequate description of the physical phenomena involved.

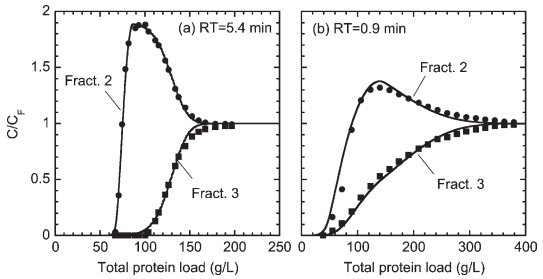

Figure 3. Two-component breakthrough curves of a mixture containing 1 g/L each of mAb Fraction 2 and 3 for UNOsphere S columns at different residence times (RT=*L/u*).

Column lengths were 55 and 23 mm for (a) and (b), respectively. Lines show predictions of the pore diffusion model with $D_e = 8.3 \times 10^{-8}$ cm^2/s.

Results for Capto S

Figure 5 shows representative batch adsorption kinetic results obtained for Capto S by Tao et al.[6] for single-component adsorption, coadsorption, and sequential adsorption. As seen from this figure, single- and two-component coadsorption occur over similar time scales (ca. 4,000 s), significantly shorter than for the corresponding UNOsphere S experiments despite the higher binding capacity and larger particle size of Capto S. These results suggest much faster mass transfer in Capto S compared to UNOsphere S. Much slower rates are obtained, however, for the sequential adsorption case (Figure 5c), when particles saturated with Fraction 2 were subsequently exposed to Fraction 3. In this case, even after 6,000 s, the process is far from completion suggesting that transport during the displacement of Fraction 2 by Fraction 3 is severely hindered.

The model used by Tao et al.[6] to describe the Capto S rate data assumed constant diffusivities and uncoupled diffusion fluxes, with the driving force written in terms of the gradient of adsorbed protein concentration $\bigtriangledown q_i$. Accordingly, the mass-transfer flux is given by

$$J_i = -D_{s,i}\nabla q_i \tag{7}$$

where $D_{s,i}$ is a Fickian surface or adsorbed-phase diffusivity, assumed to be constant. The adsorption kinetics in spherical particles is, thus, described for each component by the following equations and boundary conditions

$$\frac{\partial q_i}{\partial t} = \frac{D_{s,i}}{r^2}\frac{\partial}{\partial r}\left(r^2\frac{\partial q_i}{\partial r}\right) \tag{8}$$

$$\left.\frac{\partial q_i}{\partial r}\right|_{r=0} = 0 \tag{8a}$$

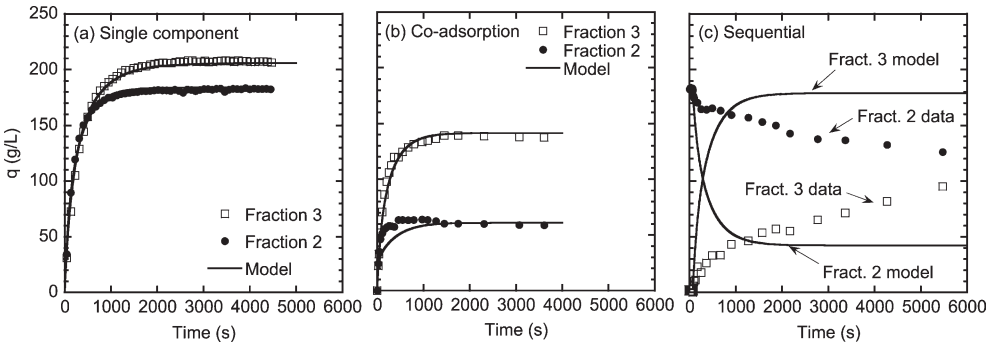

Figure 5. Batch adsorption kinetics of Capto S.

(a) Single-component adsorption of mAb Fractions 2 and 3 from 1 g/L solutions, (b) coadsorption of mAb Fractions 2 and 3 from a solution containing 1 g/L of each variant, and (c) Sequential adsorption of Fraction 3 from a 1 g/L solution of Fraction 3 on particles pre-equilibrated in a 1 g/L solution of Fraction 2. Data are from Tao et al.[6] Lines show predictions of the solid-diffusion model with constant diffusivity $D_s = 4.0 \times 10^{-9}$ cm^2/s.

$$D_{s,i}\left.\frac{\partial q_i}{\partial r}\right|_{r=r_p} = k_{f,i}\left(C_i - \frac{q_i|_{r=r_p}/q_0}{\left(K_{e,i}q_0^{z_i}/C_I^{z_i}\right)\left[1-\sum_j (z_j+\sigma_j)q_j|_{r=r_p}/q_0\right]^{z_i}}\right) \tag{8b}$$

$$V\frac{dC_i}{dt} = -\frac{3V_M}{r_p}D_{s,i}\left.\frac{\partial q_i}{\partial r}\right|_{r=r_p} \tag{9}$$

$$C_i|_{t=0} = C_{0,i} \tag{9a}$$

Model predictions obtained from these equations are shown in Figure 5, as previously presented by Tao et al.[6] with $D_s = 4.0 \times 10^{-9}$ cm^2/s. As seen in this figure the model describes both single-component and two-component adsorption kinetics with relative accuracy. However, it completely fails to describe the sequential adsorption case, predicting rates that are much faster than those observed experimentally.

The Capto S column results are shown in Figures 6 and 7 for single-component and two-component adsorption, respectively, at different residence times. For the single component case, the breakthrough curves are very steep. Correspondingly, the dynamic binding capacity at 10% of breakthrough is nearly constant, decreasing only from about 147 to about 140 g/L when the residence time is reduced from 5.2 to 0.9 min. This result is consistent with the rapid adsorption kinetics observed in the batch experiments. Model predictions obtained by coupling Eq. 8 with Eqs. 5 and 6 using the value of $D_s = 4 \times 10^{-9}$ cm^2/s determined from the batch uptake experiments are also shown in Figure 6. For this case, predictions without adjustable parameters are again in good agreement with the experimental result. Very different results are obtained, however, for two-component loading, as seen in Figure 7. In this case, despite the rapid kinetics observed for single component adsorption, there is almost no difference in the breakthrough profiles of the two variants at a 0.9 min residence time. A more substantial overshoot of Fraction 2 is obtained at a 5.2 min residence time. However, even at this longer residence time, the two variants initially coelute followed by a very long approach to column saturation with the feed mixture as Fraction 3 very slowly displaces Fraction 2. Model predictions based on Eqs. 5, 6, and 8 with $D_s = 4 \times 10^{-9}$ cm^2/s are also shown in Figure 7. Obviously the model unrealistically predicts a much more pronounced overshoot and much greater purity for the more weakly bound Fraction 2 than are observed experimentally.

The inability of the current model to predict counterdiffusion suggests that transport of multiple species in Capto S cannot be considered as occurring with either constant Fickian diffusivities or with uncoupled diffusion fluxes. A new

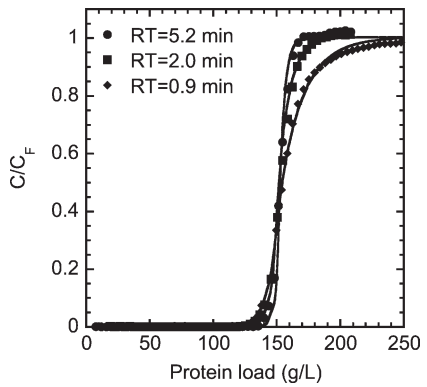

Figure 6. Single-component breakthrough curves of 2 g/L mAb Fraction 3 for a Capto S column at different residence times (RT=*L*/*u*).

The column length was 53 mm. Lines show predictions of the solid-diffusion model with constant diffusivity $D_s = 4.0 \times 10^{-9}$ cm^2/s.

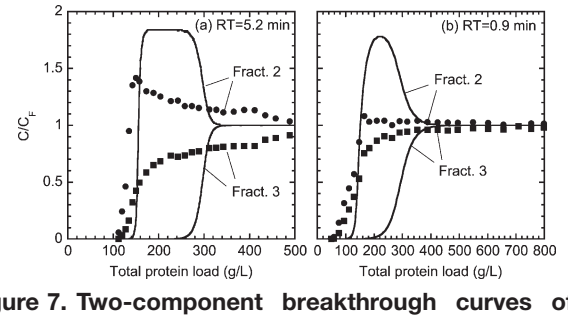

Figure 7. Two-component breakthrough curves of a mixture containing 1 g/L each of mAb Fraction 2 and 3 for Capto S columns at different residence times (RT = *L*/*u*).

Column lengths were 53 and 23 mm for (a) and (b), respectively. Lines show predictions of the solid-diffusion model with constant diffusivity $D_s = 4.0 \times 10^{-9}$ cm^2/s.

model that can consistently describe one-component, coadsorption, and sequential adsorption behavior and that can be used to predict column behavior is thus developed in the following section.

New Model Development

The kinetic behavior of Capto S resembles qualitatively the behavior observed for adsorption in zeolitic structures when the size of the adsorbate approaches the zeolite channel size. In this case, molecules cannot pass each other and transport is thought to occur through a so-called ''single-file diffusion'' (SFD) mechanism. Accordingly, diffusion is highly dependent on occupancy of the adsorption sites and is expected to decrease rapidly as a function of coverage. Several approaches have been introduced to describe these effects.[16–21] Following van den Broeke[21] multicomponent mass transfer in such pores can be described by the Maxwell-Stefan model. Accordingly, the vector of diffusion fluxes **J**, is given by

$$\mathbf{J} = -\mathbf{B}^{-1}\Gamma\nabla\mathbf{q} \tag{10}$$

where $\mathbf{B}^{-1}$ is a matrix of Maxwell-Stefan diffusivities, and Γ a matrix of thermodynamic factors expressing the relationship between the chemical potential driving force and the concentration-based driving force $\bigtriangledown\mathbf{q}$. For a two-component system comprising species A and B, neglecting cross-coefficients in the diffusivity matrix, Eq. 10 yields[21]

$$\mathbf{J} = -\begin{bmatrix} \overline{D}_{s,A}(q_A,q_B) & 0 \\ 0 & \overline{D}_{s,B}(q_A,q_B) \end{bmatrix} \begin{bmatrix} \frac{q_A}{RT}\frac{\partial\mu_A}{\partial q_A} & \frac{q_A}{RT}\frac{\partial\mu_A}{\partial q_B} \\ \frac{q_B}{RT}\frac{\partial\mu_B}{\partial q_A} & \frac{q_B}{RT}\frac{\partial\mu_B}{\partial q_B} \end{bmatrix} \nabla\mathbf{q} \tag{11}$$

where $\overline{D}_{s,i}(q_A,q_B)$ and μ_i are the Maxwell-Stefan diffusivity and the chemical potential, respectively, of component i. The former are theoretically related to ''hopping'' or migration rates,[8,21] while the latter, neglecting activity coefficients, are related to the adsorbate concentration in solution C_i, through the following equation

$$\mu_i = \mu_i^0 + RTlnC_i \tag{12}$$

Accordingly, we have

$$\frac{q_i}{RT}\frac{\partial\mu_i}{\partial q_j} = \frac{q_i}{C_i}\frac{\partial C_i}{\partial q_j} \tag{13}$$

where the partial derivatives $\partial C_i/\partial q_j$ are obtained from the adsorption isotherm. The effects of the cross-coefficients in the diffusivity matrix can be significant for certain conditions[22]. However, as discussed, by Krishna and van den Broeke[23] and Gavalas[24] these terms are usually neglected for SFD since the possibility of adsorbed molecules exchanging place is not likely. The final result in scalar form, neglecting these terms, is given by the following equations:

$$J_A = -\overline{D}_{s,A}(q_A,q_B)\frac{q_A}{C_A}\left(\frac{\partial C_A}{\partial q_A}\nabla q_A + \frac{\partial C_A}{\partial q_B}\nabla q_B\right) \tag{14}$$

$$J_B = -\overline{D}_{s,B}(q_A,q_B)\frac{q_B}{C_B}\left(\frac{\partial C_B}{\partial q_A}\nabla q_A + \frac{\partial C_B}{\partial q_B}\nabla q_B\right) \tag{15}$$

Application of the latter relationships requires both the definition of the adsorption isotherm, which appears through the partial derivatives $\partial C_i/\partial q_j$, as well as the composition dependence of the Maxwell-Stefan diffusivities $\overline{D}_{s,i}(q_A,q_B)$. For the latter van den Broeke[21] suggests two limiting cases. The first, corresponding to free surface or solid-phase diffusion, is a maximum mobility case, where the $\overline{D}_{s,i}$ values are assumed to be constant. The second case corresponds to single-file diffusion and occurs when the adsorbed molecules cannot pass each other as a result of spatial constraints introduced by the adsorbent matrix. In this case, the mobility of adsorbed molecules is dependent on the probability of an empty adjacent adsorption site. Obviously, this probability and, hence, the mobility of the adsorbed molecules, decreases as the occupancy of adsorption sites increases. The final result depends on the shape of the adsorption isotherm. Two cases are considered: the Langmuir isotherm and the SMA model.

Systems described by the Langmuir isotherm

The well-established result for the Langmuir isotherm[16–17,21] is briefly presented for comparison purposes. In this case the multicomponent isotherm is given by

$$C_i = \frac{q_i/q_m}{K_i\left(1-\sum_j\frac{q_j}{q_m}\right)} \tag{16}$$

where q_m is the ''monolayer'' binding capacity, and K_i the equilibrium constant. Equations 14 and 15 yield

$$J_A = -\frac{\overline{D}_{s,A}(q_A,q_B)}{1-\sum_j\frac{q_j}{q_m}}\left[\left(1-\frac{q_B}{q_m}\right)\nabla q_A + \frac{q_A}{q_m}\nabla q_B\right] \tag{17}$$

$$J_B = -\frac{\overline{D}_{s,B}(q_A,q_B)}{1-\sum_j\frac{q_j}{q_m}}\left[\frac{q_B}{q_m}\nabla q_A + \left(1-\frac{q_A}{q_m}\right)\nabla q_B\right] \tag{18}$$

For the SFD case, the composition dependence of the Maxwell-Stefan diffusivity is given by the following equation[21]

$$\overline{D}_{s,i}(q_A,q_B) = \overline{D}_{s,i}(0)\times P_i(q_A,q_B) \tag{19}$$

where $\overline{D}_{s,i}(0)$ is the Maxwell-Stefan diffusivity at zero coverage, and $P_i(q_A, q_B)$ is the probability of an empty nearest neighbor adsorption site. For the Langmuir isotherm, with each component occupying a single adsorption site, this probability is simply

$$P_i(q_A,q_B) = 1-\sum_j\frac{q_j}{q_m} \tag{20}$$

It can be seen that the product of eq. 20 times C_i is proportional to an adsorption rate while the term q_i/q_mK_i is proportional to a desorption rate. Equating the two rates yields Eq. 16. The final result is given by the following equations

$$J_A = -\overline{D}_{s,A}(0)\left[\left(1-\frac{q_B}{q_m}\right)\nabla q_A + \frac{q_A}{q_m}\nabla q_B\right] \tag{21}$$

$$J_B = -\overline{D}_{s,B}(0)\left[\frac{q_B}{q_m}\nabla q_A + \left(1-\frac{q_A}{q_m}\right)\nabla q_B\right] \tag{22}$$

It can be seen that these equations predict that mass transfer rates are influenced by whether adsorption takes place with one or two components and by the direction of transport radially within the particle. For a one-component system, the equivalent Fickian diffusivity $D_{s,i} = J_i/\nabla q_i = \overline{D}_{s,i}(0)$ is predicted to be a constant, independent of adsorbed concentration. For coadsorption on an initially clean adsorbent, both fluxes remain finite and transport is predicted to occur at rates similar to the one-component case. Finally, for sequential displacement, when the adsorbent is initially nearly saturated with component B and then exposed to component A, the flux of the counterdiffusing species is predicted to become vanishingly small as $q_B/q_m \to 1$ and q_A/q_m is initially zero.

Systems described by the SMA model

For the SMA model, Eqs. 1, 14, and 15 yield the following result[25]

$$J_A = -\overline{D}_{s,A}(q_A,q_B)\left[\frac{q_I + z_A(z_A+\sigma_A)q_A}{q_I}\nabla q_A + \frac{z_A(z_B+\sigma_B)q_A}{q_I}\nabla q_B\right] \tag{23}$$

$$J_B = -\overline{D}_{s,B}(q_A,q_B)\left[\frac{z_B(z_A+\sigma_A)q_B}{q_I}\nabla q_A + \frac{q_I + z_B(z_B+\sigma_B)q_A}{q_I}\nabla q_B\right] \tag{24}$$

where $q_I = q_0 - \sum\left(z_j+\sigma_j\right)q_j$ is the concentration of adsorbate-free functional groups on the ion exchanger. Since this treatment is for ion exchange, the latter are, of course, assumed to be occupied by counterions, which are present in solution in concentration C_I, in order to maintain electroneutrality. For the composition dependence of the Maxwell-Stefan diffusivities, we assume

$$\overline{D}_{s,i}\left(q_A,q_B\right) = \overline{D}_{s,i}(0)\times P_i(q_A,q_B) = \overline{D}_{s,i}(0)\times\left[1-\sum_j\left(z_j+\sigma_j\right)\frac{q_j}{q_0}\right]^{z_i} \tag{25}$$

This relationship is empirical, but can be justified as follows. For the SMA model, since each adsorbed protein occupies $z_i + \sigma_i$ functional groups, the probability $P_i(q_A, q_B)$ is less than $1-\sum_j\left(z_j+\sigma_j\right)q_j/q_m$ since not all adsorbate-free functional groups are in clusters of the required size $z_i+\sigma_i$. Unfortunately, an exact expression for P_i does not seem to exist for this case. However, a reasonable assumption is to take $P_i\left(q_A,q_B\right) = \left[1-\sum_j\left(z_j+\sigma_j\right)\frac{q_j}{q_0}\right]^{z_i}$. In this case, in the context of the SMA model, the product $C_i\times\left[1-\sum_j\left(z_j+\sigma_j\right)\frac{q_j}{q_0}\right]^{z_i}$ is proportional to the forward rate of exchange of adsorbate i for counterions, while the term $q_i C_I^{z_i}/K_e q_0^{z_i}$ is proportional to the reverse exchange rate. Equating the two rates yields Eq. 1. Thus, the assumed probability is consistent with the formalism of the SMA isotherm. Obviously, for $z_i = 1$ and $\sigma_i = 0$ (i.e., monovalent exchange without steric hindrance), Eqs. 23–25 reduce to their Langmuir counterpart (Eqs. 21 and 22). For other cases, the predicted fluxes are expected to follow trends similar to the Langmuir case, but with a quantitatively different dependence on composition. In the limit where $1-\sum_j\left(z_j+\sigma_j\right)q_j/q_0 = 0$, obtained when $C_I \to 0$, Eq. 25 predicts zero Maxwell-Stefan diffusivities. In practice, however, this does not occur in our experimental system since there is always a finite concentration of counterions associated with the buffer.

Model Predictions for Capto S

Predictions of the batch adsorption kinetics with the SFD model are obtained from the following material balances and boundary conditions:

$$\frac{\partial q_i}{\partial t} = -\frac{1}{r^2}\frac{\partial}{\partial r}\left(r^2 J_i\right) \tag{26}$$

$$\left.\frac{\partial c_i}{\partial r}\right|_{r=0} = 0 \tag{26a}$$

$$J_i|_{r=r_p} = k_{f,i}\left(C_i - \frac{q_i|_{r=r_p}\Big/q_0}{\left(K_{e,i}q_0^{z_i}/C_I^{z_i}\right)\left[1-\sum_j\left(z_j+\sigma_j\right)q_j\big|_{r=r_p}\Big/q_0\right]^{z_i}}\right) \tag{26b}$$

$$V\frac{dC_i}{dt} = -\frac{3V_M}{r_p}J_i|_{r=r_p} \tag{27}$$

$$C_i|_{t=0} = C_i^0 \tag{27a}$$

where the fluxes J_i, are given by Eqs. 23–25. Model predictions based on $\overline{D}_s(0) = 4.5\times10^{-8}$ cm^2/s, obtained by fitting the single component data for both variants and $k_f = 0.0015$ cm/s, as previously determined,[6] are shown in Figure 8. Other parameters are also as previously determined. Although the single component and two-component co-adsorption predictions are virtually the same, the $\overline{D}_s(0)$-value obtained for the SFD model (4.5×10^{-8} cm^2/s) is different from the value of D_s determined for the constant Fickian diffusivity model (Eqs. 3 and 4; $D_s = 4.0\times10^{-9}$ cm^2/s) since the two models express the flux with different driving forces. Unlike the constant Fickian diffusivity model, however, the SFD model also predicts with very reasonable accuracy the much slower rate observed for the sequential adsorption case.

Predictions of the column behavior are obtained similarly by combining Eqs. 23–25 with the column balances (Eqs. 5 and 6). The numerical solution of the corresponding equations is shown in Figure 9 also for $\overline{D}_s(0) = 4.5\times10^{-8}$ cm^2/s and $k_f = 0.0015$ cm/s for both variants. The model correctly predicts the nearly identical breakthrough curves observed experimentally for the two variants at 0.9 min residence time and the relatively small improvement in their separation obtained at 5.2 min. Although the peak concentration of Fraction 2 is somewhat underestimated, the model correctly predicts the slow approach to column saturation with the feed mixture as Fraction 3 gradually displaces Fraction 2.

Conclusions

Our previously developed pore diffusion model based on batch measurements accurately describes the single- and two-component frontal loading behavior of mAb charge

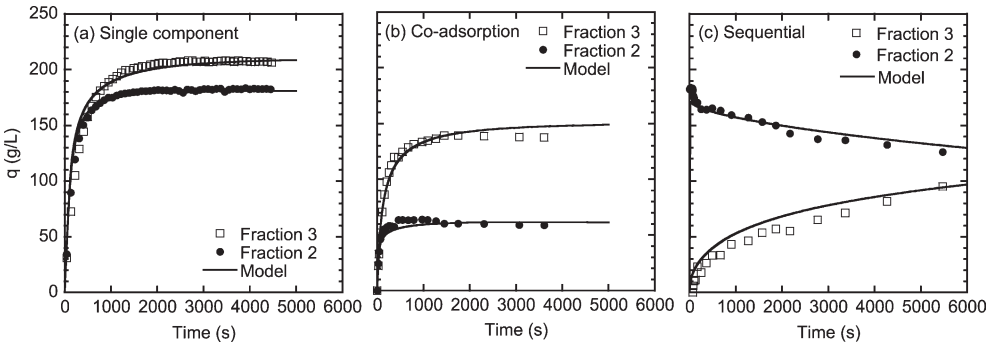

Figure 8. Batch adsorption kinetics of Capto S. Data from Figure 5.

Lines show predictions of the SFD model with $\overline{D}_s/0 = 4.5 \times 10^{-8}$ cm^2/s.

variants for columns packed with the macroporous stationary phase UNOsphere S over a broad range of residence times and with different feed compositions. In this case, diffusion in the particle pores with an apparently rapid exchange of adsorbed mAb molecules is principally responsible for the breadth of single and two-component breakthrough curves as a function of residence time. The effective pore diffusivity for the mAb variants in this matrix is $D_e = 8.3 \times 10^{-8}$ cm^2/s. Since the free solution diffusivity is $D_0 \sim 4 \times 10^{-7}$ cm^2/s,[26] we obtain $D_e/D_0 \sim 0.2$, a value that suggests relatively low-diffusional hindrance.[27]

A new model was developed to describe single and two-component adsorption in Capto S. Because of the very small accessible pore size, counterdiffusion of different charge variants appears to be severely hindered and occurs over time scales that are much longer than those of single-component adsorption and two-component coadsorption. The new model is based on the Maxwell-Stefan equations and assumes single-file diffusion. Accordingly, we assume that mAb molecules are not able to diffuse past the adsorbed ones within the dextran grafts leading to apparent Fickian diffusivities that decrease as the adsorbed protein concentration increases. The new model correctly predicts fast adsorption kinetics for single component adsorption and two-component coadsorption, but very slow transport for sequential adsorption, when a more strongly bound variant displaces a more weakly bound one. Without adjustable parameters, the SFD model also provides an approximate prediction of the single- and two-component column behavior. The latter exhibits nearly identical breakthrough curves for the two variants at short residence times as a result of the slow counterdiffusion process predicted by the SFD model. A final consideration regards the choice of the model for practical calculations. It is apparent that the pore diffusion model is appropriate for macroporous adsorbents. Further simplifications are possible in this case to predict column behavior for both single and multicomponent systems using a linear-driving-force (LDF) rate model in lieu of the particle diffusion model used in this work as discussed, for example, in LeVan and Carta.[28] On the other hand, for adsorbents such as Capto S, where multicomponent mass transfer fluxes appear to be coupled, predictions with simple LDF-rate models are likely to be inaccurate, since in this case, transport rates vary widely with the direction of transport. Simplified models may, however, be developed based on the so-called "film model approximation" which has been shown appropriate even when the intraparticle diffusivity is not constant and diffusion fluxes are coupled.[15,29]

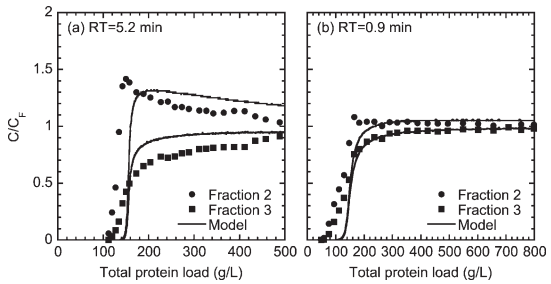

Figure 9. Two-component breakthrough curves for Capto S. Data from Figure 7.

Lines show predictions of the SFD model with $\overline{D}_s/0 = 4.5 \times 10^{-8}$ cm^2/s.

Acknowledgments

This research was supported by MedImmune and NSF Grant No. CBET-1032727.

Notation

Symbols

Bi = Biot number, $= k_f r_p/D_e$
c = protein concentration in the particle pores, mmol/L or g/L
C = protein concentration in solution, mmol/L or g/L
C_F = feed protein concentration, mmol/L or g/L
C_I = concentration of counterions in solution, mmol/L
C_0 = initial protein concentration in solution, mmol/L or g/L
D_e = effective pore diffusivity in pore diffusion model, cm^2/s
D_s = adsorbed phase diffusivity in solid diffusion model, cm^2/s
$\overline{D}_s$ = Maxwell-Stefan diffusivity, cm^2/s
D_0 = free solution diffusivity, cm^2/s
J = mass-transfer flux, mmol/cm^2 s or g/cm^2 s
k_f = boundary layer film mass-transfer coefficient, cm/s
K = equilibrium constant in Langmuir isotherm model, L/mmol or L/g
K_e = equilibrium constant in SMA model
L = column length, cm
q = adsorbed protein concentration, mmol/L or g/L
q_I = concentration of unoccupied charged groups in stationary phase, mmol/L
$\overline{q}$ = particle-average adsorbed protein concentration, mmol/L or g/L
q_m = binding capacity, mmol/L or g/L
q_0 = concentration of charged functional groups, mmol/L
r_p = particle radius, cm
R = gas law constant, J/mol K
RT = residence time, $= L/u$, s
t = time, s
T = absolute temperature, K
u = superficial velocity, cm/s
V = solution volume, L
V_M = volume of stationary phase, L
x = column axial coordinate, cm
z = protein effective charge in SMA model

ε = extraparticle column void fraction
μ = chemical potential, J/mol
σ = steric hindrance parameter in SMA model

Literature Cited

1. Gottschalk U, *Process scale purification of antibodies*. Hoboken: John Wiley & Sons, Inc; 2009.
2. Weitzhandler W, Farnan D, Horvath J, Rohrer JS, Slingsby RW, Advalovic N, Pohl C. Protein variant separations by cation-exchange chromatography on tentacle-type polymeric stationary phases. *J Chromatogr A*. 1998;828:365–372.
3. Harris J, Kabakoff B, Macchi FD, Shen FJ, Kwong M, Andya JD, Shire SJ, Bjork N, Totpal K, Chen AB. Identification of multiple sources of charge heterogeneity in a recombinant antibody. *J Chromatogr B*. 2001;752:233–245.
4. Melter L, Ströhlein G, Butté A, Morbidelli M. Adsorption of monoclonal antibody variants on analytical cation-exchange resin. *J Chromatogr A*. 2007;1154:121–131.
5. Tao Y, Carta G, Ferreira G, Robbins D. Adsorption of deamidated antibody variants on macroporous and dextran-grafted cation exchangers: I. Adsorption equilibrium. *J Chromatogr A*. 2011; 1218:1519–1529.
6. Tao Y, Carta G, Ferreira G, Robbins D. Adsorption of deamidated antibody variants on macroporous and dextran-grafted cation exchangers: II. Adsorption kinetics. *J Chromatogr A*. 2011;1218: 1530–1537.
7. Wesselingh JA, Bosma JC. Protein ion-exchange adsorption kinetics. *AIChE J*. 2001;47:1571–1580.
8. Lenhoff AM, Multiscale modeling of protein uptake patterns in chromatographic particles. *Langmuir*. 2008;24:5991–5995.
9. Carta G, Ubiera AR, Pabst TM. Protein mass transfer kinetics in ion exchange media: Measurements and interpretations. *Chem Eng Technol*. 2005:1252–1264.
10. Tao Y, Perez Almodovar EX, Carta G, Ferreira G, Robbins D. Adsorption of deamidated antibody variants on macroporous and dextran-grafted cation exchangers: III. Microscopic studies. *J Chromatogr. A*. 2011;1218:8027–8035.
11. Hagel L, Ostberg M, Andersson T. Apparent pore size distributions of chromatography media. *J Chromatogr A*. 1996;743:33–42.
12. Brooks CA, Cramer SM. Steric mass-action ion-exchange - displacement profiles and induced salt gradients. *AIChE J*. 1992;38:1969–1978.
13. Ruthven DM. *Principles of adsorption and adsorption processes*. New York: John Wiley & Sons, Inc; 1984.
14. Carta G, Jungbauer A. *Protein Chromatography - Process Development and Scale-up*. Weinheim: Wiley-VCH; 2010.
15. Carta G, Lewus RK. Film model approximation for particle-diffusion-controlled multicomponent ion exchange. *Sep Sci Technol*. 1999;34:2685–2697.
16. Qureshi WR, Wei J. One-component and 2-component diffusion in zeolite ZSM-5. 1. Theoretical. *J Catal*. 1990;126:126–146.
17. Qureshi WR, Wei J. One-component and 2-component diffusion in zeolite ZSM-5. 2. Experimental. *J Catal*. 1990;126:147–172.
18. Tsikoyiannis JG, Wei J. Diffusion and reaction in high-occupancy zeolite catalysts. 1. A stochastic-theory. *Chem Eng Sci*. 1991;46: 233–253.
19. Dahlke K, Emig G. Diffusion in Zeolites - a random-walk approach. *Catal Today*. 1991;8:439–450.
20. Wei J. Nonlinear phenomena in zeolite diffusion and reaction. *Ind Eng Chem. Res*. 1994;33:2467–2472.
21. van den Broeke LJP. Simulation of diffusion in zeolitic structures. *AIChE J*. 1995;41:2399–2414.
22. van de Graaf JM, Kapteijn F, Moulijn JA. Modeling permeation of binary mixtures through zeolite membranes. *AIChE J*. 1999;45:497–511.
23. Krishna R, van den Broeke LJP. Maxwell-Stefan description of mass transport across zeolite membranes. *Chem Eng J*. 1995;57: 155–162.
24. Gavalas GR. Diffusion in microporous membranes: measurements and modeling. *Ind Eng Chem Res*. 2008;47:5797–5811
25. Lewus RK, Carta G. Binary protein adsorption on gel-composite ion-exchange media. *AIChE J*. 1999;45:512–522.
26. Tyn MT, Gusek TW. Prediction of diffusion coefficients of proteins. *Biotechnol. Bioeng*. 1990;35:327–338.
27. Cussler EL. *Diffusion: mass transfer in fluid systems*. 2nd ed. Cambridge: Cambridge University Press; 1997.
28. LeVan MD, Carta G. *Adsorption and Ion Exchange*. In: Green DW, Ed. *Perry's Chemical Engineers Handbook. Section 16*. 8th ed. New York: McGraw-Hill; 2007.
29. Carta G, Lewus RK. Film model approximation for multicomponent adsorption. *Adsorption*. 2000;6:5–13.

Manuscript received Aug. 24, 2011, and revision received Nov. 30, 2011.